The Astrophysical Journal, 863:121 (8pp), 2018 August 20 https://doi.org/10.3847/1538-4357/aad283

A Projected Estimate of the Reionization Optical Depth Using the CLASS Experiment's Sample Variance Limited E-mode Measurement

Duncan J. Watts[1], Bingjie Wang (王冰洁)[1], Aamir Ali[1,2], John W. Appel[1], Charles L. Bennett[1], David T. Chuss[3], Sumit Dahal (सुमित दाहाल)[1], Joseph R. Eimer[1], Thomas Essinger-Hileman[4], Kathleen Harrington[1], Gary Hinshaw[5], Jeffrey Iuliano[1], Tobias A. Marriage[1], Nathan J. Miller[1,4], Ivan L. Padilla[1], Lucas Parker[1,6], Matthew Petroff[1], Karwan Rostem[4], Edward J. Wollack[4], and Zhilei Xu (徐智磊)[1,7]

[1] Department of Physics and Astronomy, Johns Hopkins University, 3701 San Martin Drive, Baltimore, MD 21218, USA; dwatts@jhu.edu
[2] Department of Physics, University Of California, Berkeley, CA 94720, USA
[3] Department of Physics, Villanova University, 800 Lancaster Avenue, Villanova, PA 19085, USA
[4] Goddard Space Flight Center, 8800 Greenbelt Road, Greenbelt, MD 20771, USA
[5] Department of Physics and Astronomy, University of British Columbia, 6224 Agricultural Road, Vancouver, BC V6T 1Z1, Canada
[6] Space and Remote Sensing, MS D436, Los Alamos National Laboratory, Los Alamos, NM 87544, USA
[7] Department of Physics and Astronomy, University of Pennsylvania, 209 South 33rd Street, Philadelphia, PA 19104, USA
Received 2018 January 4; revised 2018 June 21; accepted 2018 July 8; published 2018 August 16

Abstract

We analyze simulated maps of the Cosmology Large Angular Scale Surveyor (CLASS) experiment and recover a nearly cosmic variance limited estimate of the reionization optical depth τ. We use a power spectrum-based likelihood to simultaneously clean foregrounds and estimate cosmological parameters in multipole space. Using software specifically designed to constrain τ, the amplitude of scalar fluctuations A_s, and the tensor-to-scalar ratio r, we demonstrate that the CLASS experiment will be able to estimate τ within a factor of two of the cosmic variance limit allowed by full-sky cosmic microwave background polarization measurements. Additionally, we discuss the role of CLASS's τ constraint in conjunction with gravitational lensing of the CMB on obtaining a $\gtrsim 4\sigma$ measurement of the sum of the neutrino masses.

Key words: cosmic background radiation – cosmological parameters – early universe – gravitational waves – inflation

1. Introduction

Measurements of the cosmic microwave background (CMB) have tightly constrained the properties of the large-scale observable universe, with the reionization optical depth τ left as the worst-determined fundamental ΛCDM parameter (Bennett et al. 2013; Planck Collaboration et al. 2016c). The importance of polarization measurements has become more critical as the *Planck* experiment has measured the unpolarized temperature anisotropy over the full sky to its sample variance limit up to a resolution of $\theta \gtrsim 7'$ ($\ell \lesssim 1600$) (Section 3.8 of Leenaarts et al. 2016, albeit with potential complications, see Addison et al. 2016). At sub-degree angular scales ($\ell \gtrsim 200$), polarization power is sourced by primordial scalar fluctuations with extra correlations induced by gravitational lensing (e.g., Hu & Okamoto 2004; Galli et al. 2014; Louis et al. 2017; Henning et al. 2018). At larger angular scales, gradient-like E-mode polarization measurements can tightly constrain the reionization optical depth τ via the rough scaling $C^{\rm EE}_{2\leqslant\ell\leqslant 20} \propto \tau^2$ (Page et al. 2007), while we can use the curl-like B-mode polarization measurements to constrain the amplitude of stochastic gravitational waves that the inflationary paradigm predicts, whose amplitude is parameterized by the ratio r of tensor-to-scalar fluctuations in the metric (Kazanas 1980; Starobinsky 1980; Einhorn & Sato 1981; Guth 1981; Mukhanov & Chibisov 1981; Albrecht & Steinhardt 1982; Linde 1982; Kamionkowski et al. 1997; Seljak & Zaldarriaga 1997). The CLASS experiment is uniquely and specially designed to constrain r and τ by recovering the largest scale fluctuations of the polarized CMB across 70% of the sky (Eimer et al. 2012; Essinger-Hileman et al. 2014; Harrington et al. 2016).

The reionization optical depth τ is the total free electron opacity to the surface of last scattering,

$$\tau = \int_{t_{\rm lss}}^{t_0} n_{\rm e}(t)\sigma_{\rm T} c\, dt, \tag{1}$$

where $n_{\rm e}(t)$ is the average number density of free electrons from the time of last scattering $t_{\rm lss}$ to today t_0 and $\sigma_{\rm T}$ is the Thomson scattering cross section. For $\tau \ll 1$, the reionization optical depth is the probability that a CMB photon was scattered by free electrons from reionization. The redshift of reionization can be defined if one assumes that $n_{\rm e}(t)$ is nearly a step function, but it is likely that reionization was an extended process, with evidence of significant contributions to τ up to $z \sim 16$ (Heinrich et al. 2017).

From measurements of QSO absorption lines via the Gunn–Peterson effect (Gunn & Peterson 1965), we know that the universe was ionized by redshift $z = 6$, corresponding to a lower limit of $\tau \gtrsim 0.038$ if we assume instantaneous reionization (Fan et al. 2006; Planck Collaboration et al. 2016a). The quantity τ can be constrained using measurements of the temperature-E-mode cross-correlation and the E-mode auto-correlation $C_\ell^{\rm TE}$ and $C_\ell^{\rm EE}$ at the largest angular scales. The *Planck* and *WMAP* measurements are limited in precision by sample variance in the $C_\ell^{\rm TE}$ case, and by instrumental noise and systematic effects in the $C_\ell^{\rm EE}$ case, with the latest limits from *Planck* giving $\tau \sim 0.06 \pm 0.01$ (Planck Collaboration et al.

2016a, 2016d) although the amplitude of unexplained large-scale signals in the *Planck* maps create extra uncertainty and potential biases in this measurement (Weiland et al. 2018). It is possible to obtain this constraint using only temperature anisotropy, CMB lensing, and baryon acoustic oscillation (BAO) data as an independent check. In particular, `PlanckTT +lensing+BAO` data constrain $\tau = 0.067 \pm 0.016$ (Planck Collaboration et al. 2016c, Section 3.4) and `WMAPTT+ lensing+BAO` data imply $\tau = 0.066 \pm 0.02$ (Weiland et al. 2018, Section 5). These constraints are independent of CMB polarization data.

Free streaming of massive neutrinos reduces the amplitude of matter fluctuations at small scales. For testing extensions to ΛCDM, a measurement of τ is necessary to reduce degeneracies between the clustering amplitude at $8\,h^{-1}$ Mpc, the physical cold dark matter density, and the sum of the neutrino masses (σ_8, $\Omega_c h^2$, and $\sum m_\nu$, respectively) (Allison et al. 2015; Liu et al. 2016). The measurement of neutrino masses is especially tantalizing since current upper limits are only a few standard deviations away from the lower limit implied by solar neutrino oscillation measurements (Abazajian et al. 2016).

The relevant polarized foregrounds, thermal dust, and synchrotron emission, dominate at large scales with their angular power spectra approximated by power laws $C_\ell^{\rm dust} \propto \ell^{-2.53}$ and $C_\ell^{\rm sync} \propto \ell^{-2.44}$ (Planck Collaboration et al. 2016b, Table 11, $f_{\rm sky}^{\rm eff} = 0.73$) and are highly anisotropic at large scales, with their minimum in frequency space falling around 70–90 GHz (Krachmalnicoff et al. 2016; Planck Collaboration et al. 2016b, Figure 51). This contamination can be mitigated by making high signal-to-noise measurements of the CMB at degree scales and cleaning foregrounds in multipole space, which is the strategy of the ACTPol (Thornton et al. 2016), BICEP (Wu et al. 2016), POLARBEAR (Suzuki et al. 2016), and SPTPol (Austermann et al. 2012) experiments. Another approach is to focus on large-scale ($\theta \gtrsim 10^\circ$) fluctuations where it is computationally simpler to remove spatially varying foregrounds in map space, an approach that has been employed using maps smoothed to $\theta \sim 15^\circ$ (Bennett et al. 2013; Leenaarts et al. 2016). For power spectrum-based analyses, the incomplete sky causes issues both due to E → B mixing (caused by spherical harmonics no longer forming a complete orthonormal basis) and the related issue that estimates of the CMB power spectrum $\hat{C}_\ell$ are not drawn from a well-understood statistical distribution. These issues have been addressed by using C_ℓ estimators that can reduce or specifically forbid E → B mixing (Chon et al. 2004; Smith & Zaldarriaga 2007, respectively), and the development of approximate likelihoods that include any potential mixing effects explicitly (Hamimeche & Lewis 2008; Mangilli et al. 2015).

Watts et al. (2015) demonstrated that the CLASS experiment, and other experiments with multifrequency data and large observing area (e.g., LSPE, Aiola et al. 2012, GroundBird, Tajima et al. 2012 and PIPER, Gandilo et al. 2016), will be able to overcome partial-sky E → B-mode mixing and known sources of foreground contamination by using an exact pixel-based likelihood for low-resolution measurements and a pseudo-C_ℓ likelihood for higher-resolution measurements. In this paper, we address mode mixing by fitting the model to the data using a pseudo-C_ℓ estimate from `PolSpice` (Chon et al. 2004) and fitting the data to theory using the approximate Wishart distribution described in Hamimeche & Lewis (2008).

Another major obstacle to characterizing large angular scales is mitigating systematic effects due to observations made on long timescales due to instrumental variations. To reach the necessary instrumental stability, a front-end modulator in the form of a variable-delay polarization modulator (VPM, Chuss et al. 2012) is used as the first optical element of each CLASS telescope (Eimer et al. 2012). This reduces instrumental effects well below the amplitude of an $r = 0.01$ signal (Miller et al. 2016).

This paper expands on Watts et al. (2015) by characterizing the estimated power spectrum across the entire angular range ($2 \leqslant \ell \leqslant 100$) while simultaneously constraining τ, A_s, r, and foreground emission, assuming $1/f$ noise reduction to $r \ll 0.01$ levels using a VPM (Miller et al. 2016). In addition to quantifying the expected cosmological parameter constraints from the full CLASS data set, we also discuss constraints using combinations from external data sets. CLASS will make a sample variance limited measurement of E-modes on the largest angular scales. With this precise measurement of τ ($\sigma_\tau \sim 0.003$), the CLASS experiment's measurements will break the $A_s e^{-2\tau}$ partial degeneracy found in temperature anisotropy measurements. The resulting improved constraint on A_s enables tighter bounds on the sum of neutrino masses $\sum m_\nu$.

In Section 2, we will discuss our simulated data and the assumptions that go into our modeling. Section 3 introduces our implementation of the Hamimeche & Lewis (2008) pseudo-C_ℓ likelihood and its efficacy at providing constraints given the simulated data. Section 4 discusses the implications of a CLASS τ measurement in the context of external cosmological parameter constraints. Unless noted otherwise, all cosmological parameters are those listed in Planck Collaboration et al. (2016a), specifically `PlanckTTTEEE +SIMlow`.

2. Simulated Maps

We use the CLASS instrument and survey specifications for our simulated data as enumerated in Essinger-Hileman et al. (2014). The CLASS experiment is located in the Atacama Desert in Chile, at a latitude of −23°, scanning 70% of the sky every day at 45° elevation. We combine a mask due to the survey geometry with the *WMAP* P06 Galactic foreground mask, which cuts out the brightest 25% of the sky (Page et al. 2007). This leaves CLASS with an observed sky fraction of $f_{\rm sky} = 0.47$. The CLASS frequency bands are chosen to minimize atmospheric emission while straddling the Galactic foreground minimum. Assuming a 5 year survey with 40, 90, 150, and 220 GHz channels, the maps are assigned weights per pixel $w_{p,\nu}$, corresponding to white noise levels $w_{p,\nu}^{-1/2} = [39, 10, 15, 43]$ μK arcmin. We use this to simulate maps of white noise as draws of a Gaussian random variable $\boldsymbol{n}^\nu \sim \mathcal{N}(0, \sigma_\nu^2 \boldsymbol{I})$ with $\sigma_\nu = w_{p,\nu}^{-1/2} \big/ \sqrt{\Omega_{\rm pix}}$, where $\Omega_{\rm pix}$ is the area of a `HEALPix` pixel at the simulated resolution, here $N_{\rm side} = 128$.[8]

We simulate foreground emission using `PySM` (Thorne et al. 2017),[9] which takes into account polarized foreground measurements from *Planck* and *WMAP* (polarized dust from Planck Collaboration et al. 2016b, polarized synchrotron from

[8] `HEALPix` (Górski et al. 2005) maps are divided into $12N_{\rm side}^2$ pixels, with each pixel width $\theta_{\rm pix} \sim 58.^\circ 6/N_{\rm side}$. The full documentation can be found at http://healpix.sourceforge.net.

[9] https://github.com/bthorne93/PySM_public

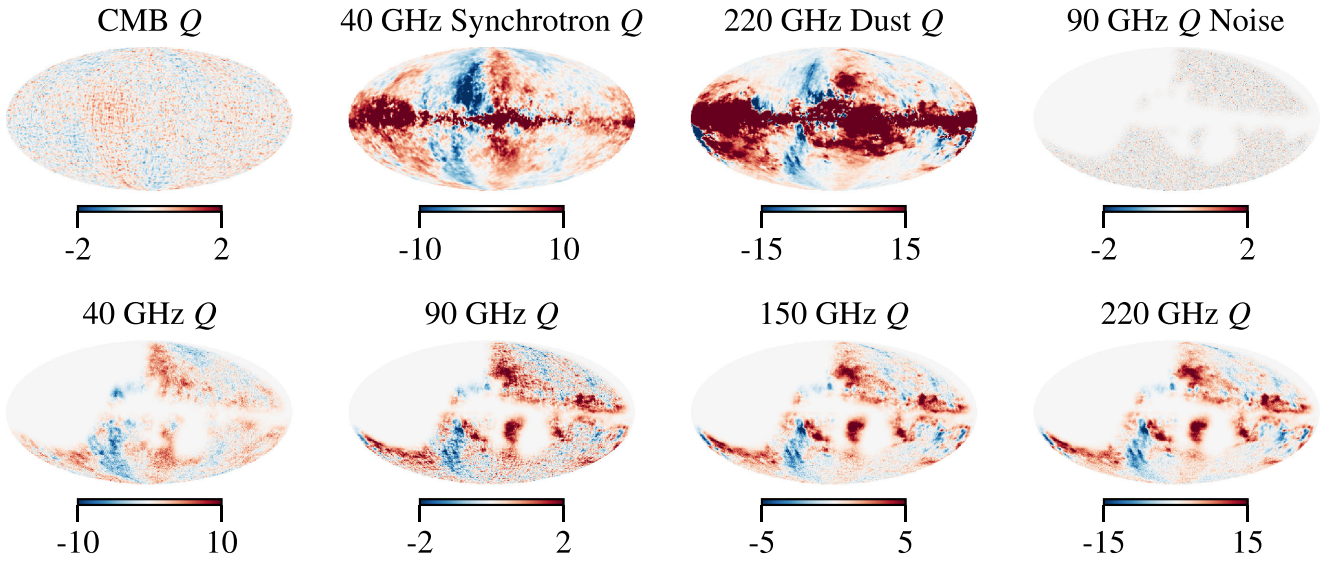

Figure 1. Simulated CLASS maps include a realization of the CMB, polarized synchrotron and thermal dust emission, and Gaussian white noise. The top panels show the individual Stokes Q components of the simulation, while the bottom show the simulated multifrequency Stokes Q CLASS maps, with the Galactic plane masked and parts of the celestial Northern Hemisphere and celestial Southern Hemisphere excluded by the survey boundary. All maps are displayed in Galactic coordinates with units of μK.

Bennett et al. 2013). While it is known that the emission laws of these foregrounds vary across the sky, with antenna temperature emission parameterized as

$$\boldsymbol{m}^{\nu}_{\rm sync} = \boldsymbol{m}_{\rm sync}\left(\frac{\nu}{\nu_{\rm S}}\right)^{\beta_{\rm S}(\hat{\boldsymbol{n}})}$$
$$\boldsymbol{m}^{\nu}_{\rm dust} = \boldsymbol{m}_{\rm dust}\left(\frac{\nu}{\nu_{\rm D}}\right)^{\beta_{\rm D}(\hat{\boldsymbol{n}})-2}\frac{B_{\nu}[T_{\rm D}(\hat{\boldsymbol{n}})]}{B_{\nu_{\rm D}}[T_{\rm D}(\hat{\boldsymbol{n}})]}, \quad (2)$$

current data do not yet meaningfully constrain the spatial variation of spectral indices within our sky cut (Watts et al. 2015 Appendix B, Sheehy & Slosar 2018; Planck Collaboration et al. 2018). Therefore, we model foreground emission with fixed (i.e., isotropic) synchrotron spectral index $\beta_{\rm S}$, dust spectral index $\beta_{\rm D}$, and blackbody emission $B_{\nu}[T_{\rm D}]$ with dust temperature $T_{\rm D}$. Here we use $\nu_{\rm S} = 40$ GHz and $\nu_{\rm D} = 220$ GHz as the reference frequencies, with $\boldsymbol{m}_{\rm sync}$ and $\boldsymbol{m}_{\rm dust}$ the synchrotron and dust emission at these respective frequencies. The typical levels for these parameters are $\beta_{\rm S} \sim -3.0 \pm 0.1$ (Fuskeland et al. 2014, *WMAP* intensity measurements), $\beta_{\rm D} \sim 1.6 \pm 0.1$ (Planck Collaboration et al. 2017, *Planck* polarization measurements), and $T_{\rm D} \sim 22 \pm 8$ K (Planck Collaboration et al. 2016b, *Planck* intensity measurements). While varying foreground emission laws are a significant source of bias for B-mode measurements, E-modes are much brighter and are largely unaffected by this source of uncertainty. Additionally, we addressed this complication in Watts et al. (2015) by splitting the sky up into subregions with constant emission parameters and showed that a 95% C. L. measurement of $r = 0.01$ was still possible. We have performed several simulations using the levels of spectral index variation in Thorne et al. (2017; $\Delta\beta_{\rm D} < 0.1$, $\Delta\beta_{\rm S} \sim 0.1$) and found shifts in the recovery of τ on the order of $\lesssim 0.5\sigma_{\tau}$. These simulations used a single set of foreground maps that assumed instrumental white noise. For this work, we use $\beta_{\rm D} = 1.6$ and $\beta_{\rm S} = -3$ fixed across the sky.

For the CMB signal, we use the `CAMB` package (Lewis et al. 2000)[10] to generate theoretical $C_{\ell}^{\rm EE}$ and $C_{\ell}^{\rm BB}$, keeping all parameters fixed to the `PlanckTTTEEE+SIMlow` Planck Collaboration et al. (2016a) parameters, namely $\tau = 0.0596$ and $\ln(10^{10}A_s) = 3.056$, with the addition of tensor B-modes of amplitude $r = 0.05$. With these theoretical power spectra in hand, we simulate maps using `HEALPix`'s `synfast` function, from which we take the output Q and U Stokes parameters, denoted by the vector $\boldsymbol{m}_{\rm CMB}$.

The CLASS 40, 90, 150, and 220 GHz bands have beam full width half maxima (FWHMs) of 90, 40, 24, and 18 arcmin, respectively, but for the purposes of this study we simulate the maps with a common resolution of 1.°5. We bring all of the foregrounds and CMB to this common resolution $\theta_{\rm FWHM} = 1.^{\circ}5$ and model the Gaussian noise as uncorrelated between pixels.

The data are from our multifrequency simulations

$$\boldsymbol{m}^{\nu} = g(\nu)\boldsymbol{m}^{\nu}_{\rm sync} + g(\nu)\boldsymbol{m}^{\nu}_{\rm dust} + \boldsymbol{m}_{\rm CMB} + \boldsymbol{n}^{\nu}, \quad (3)$$

where $g(\nu) \equiv \partial T/\partial T_A = (e^x - 1)^2/(x^2 e^x)$ is the conversion factor from antenna to thermodynamic temperature referenced to the CMB radiation, with $x \equiv h\nu/kT_{\rm CMB} = \nu/(56.78\ {\rm GHz})$, and $\boldsymbol{m}^{\nu}_{\rm sync/dust}$ as defined in Equation (2). A single realization of the CLASS Stokes Q maps using this prescription is shown in Figure 1.

3. Analysis Techniques

For the CLASS experiment, E-modes are far into the signal-dominated regime, with the main impediment to CMB characterization being the Galactic foreground emission (assuming all systematic measurement errors are under control). To estimate the linearly polarized Stokes parameters of the CMB maps and their polarized power spectra $C_{\ell}^{\rm EE}$ and $C_{\ell}^{\rm BB}$, we take linear combinations of the multifrequency maps constrained to keep the CMB amplitude consistent with

[10] http://camb.info

blackbody emission,

$$\hat{\boldsymbol{m}}_{\rm CMB} \equiv \sum_\nu c_\nu \boldsymbol{m}^\nu, \qquad \sum_\nu c_\nu = 1. \tag{4}$$

We ensure that the coefficients c_ν reduce foregrounds by imposing Gaussian priors

$$\sum_\nu c_\nu g(\nu) \left(\frac{\nu}{\nu_{\rm S}}\right)^{\beta_{\rm S}} = 0 \pm 0.01, \tag{5}$$

$$\sum_\nu c_\nu g(\nu) \left(\frac{\nu}{\nu_{\rm D}}\right)^{\beta_{\rm D}-2} \frac{B_\nu[T_{\rm D}]}{B_{\nu_{\rm D}}[T_{\rm D}]} = 0 \pm 0.01, \tag{6}$$

corresponding to priors on $\Delta\beta_{\rm S/D} < 0.1$. This prior down-weights unphysical solutions corresponding to values of $\beta_{\rm S/D}$ that are ruled out by existing data. This prior is relatively weak compared to the constraining power of the experiment, which returns constraints corresponding to $\Delta\beta_{\rm S} = 0.02$ and $\Delta\beta_{\rm D} = 0.005$. If the c_ν are chosen such that there are no foreground residuals while the instrumental noise contribution is minimized, the resulting power spectrum estimate will be given by

$$\hat{C}_\ell^{\rm EE/BB} = C_\ell^{\rm EE/BB} + \sum_\nu c_\nu^2 N_\ell^\nu, \tag{7}$$

where $N_\ell^\nu = w_{p,\nu}^{-1}$, in units of $\mu{\rm K}^2$ sr.

For our purposes, the foreground coefficients c_ν are nuisance parameters that are marginalized over, while the true parameters of interest are r, τ, and A_s. To account for any spurious correlations between foregrounds and CMB fluctuations, we simultaneously fit for the foreground coefficients and the cosmological parameters. Given the power spectrum estimate $\hat{C}_\ell(c_\nu)$, the noise power spectrum $N_\ell = \sum_\nu c_\nu^2 N_\ell^\nu$, and the theoretical power spectrum $C_\ell(r, A_s, \tau)$, the cut-sky likelihood for the power spectra $C_\ell^{\rm EE/BB}$ is given by minimizing

$$-2\ln\mathcal{L} \simeq \sum_{\ell\ell'} \left[G\left(\frac{\hat{C}_\ell}{C_\ell + N_\ell}\right) C_{f\ell} \right] [M_f^{-1}]_{\ell\ell'} \times \left[C_{f\ell'} G\left(\frac{\hat{C}_{\ell'}}{C_{\ell'} + N_{\ell'}}\right) \right] + 2\sum_\ell \ln|\hat{C}_\ell|, \tag{8}$$

where $G(x) \equiv \sqrt{2(x - \ln x - 1)}$. The subscript f refers to some fiducial model, and $\boldsymbol{M}_f$ is the covariance of $\hat{C}_\ell$ evaluated for the fiducial model $C_{f\ell}$ (Equation (50) of Hamimeche & Lewis 2008, see the Appendix for an explanation of the final term). We split the covariance matrix into two terms, one with CMB and white noise, and another with foreground residuals, $\boldsymbol{M}_f \equiv \boldsymbol{M}_f^{\rm C+N} + \boldsymbol{M}_f^{\rm fore}$. We estimate $\boldsymbol{M}_f^{\rm C+N}$ using simulated data on a cut sky with only CMB and Gaussian white noise contributions, using $r = 0.05$, $\ln(10^{10}A_s) = 3.056$, $\tau = 0.0596$, and $w_p^{-1/2} = 14$ μK arcmin as the fiducial model parameters. The estimated covariance matrix has $M_{f,(\ell,\ell+1)}^{\rm C+N}/M_{f,(\ell,\ell)}^{\rm C+N} \lesssim 0.1$, with most values <0.03 at the 68% C.L. The diagonal elements $M_{f,\ell\ell}^{\rm C+N}$ agree with the analytical prediction from Chon et al. (2004) at the 5% level,

$$M_{f,(\ell\ell)}^{\rm C+N} = \frac{2}{(2\ell+1) f_{\rm sky}\, w_2^2/w_4} C_\ell^2, \tag{9}$$

where $w_n = \int w(\hat{\boldsymbol{n}})^n\, d\Omega$, $w(\hat{\boldsymbol{n}})$ is the apodized mask, and $f_{\rm sky} = w_1$ is the observed sky fraction.

The addition of a term $\boldsymbol{M}_f^{\rm fore}$ accounts for any foreground residuals encountered during the fits. In principle, the best-fit solution does not have any foreground contribution, but any variation around this point in parameter space will affect the best-fit value and will potentially induce spurious correlations. To estimate the effect of foreground residuals, we took the c_ν of a successful MCMC chain without any foreground covariance accounted for and computed $\hat{C}_\ell$ of foreground residuals taken from multifrequency maps without noise or CMB. This gave a sample covariance matrix $\boldsymbol{M}_f^{\rm fore}$. Using this, we recomputed the Monte Carlo chain using this extra covariance, and found that the recovered cosmological parameters were accurately reconstructed, with an increase in their uncertainty, e.g., for the chain used in Figure 2, $\sigma_r = 0.0048 \rightarrow 0.0064$ and $\sigma_\tau = 0.0022 \rightarrow 0.0029$.

We estimate the pseudo-C_ℓ power spectrum using `PolSpice` (Chon et al. 2004), which corrects for the effects of masking and inter-bin correlations induced by the incomplete sky. We represent the estimation of the power spectrum using a bilinear operator P such that $\hat{C}_\ell = \boldsymbol{m}^T \mathsf{P} \boldsymbol{m}$. In practice, we use the bilinear property of this operator to take sums of all multifrequency cross-spectra and subtract foregrounds in multipole space, i.e.,

$$\hat{C}_\ell = \left(\sum_{\nu_1} c_{\nu_1} \boldsymbol{m}^{\nu_1}\right)^T \mathsf{P} \left(\sum_{\nu_2} c_{\nu_2} \boldsymbol{m}^{\nu_2}\right) = \sum_{\nu_1,\nu_2} c_{\nu_1} c_{\nu_2} \hat{C}_\ell^{\nu_1\times\nu_2}, \tag{10}$$

where we have defined $\hat{C}_\ell^{a\times b} \equiv (\boldsymbol{m}^a)^T \mathsf{P} \boldsymbol{m}^b$.

The method outlined here reduces and accounts for any E $\rightarrow$ B mixing inherent in the analysis of an incomplete sky while accounting for the underlying statistical distribution of the power spectrum. `PolSpice` returns a decoupled estimate of the polarization power spectra, giving an unbiased estimate of the true underlying power spectrum while minimizing spurious correlations between E-modes and B-modes. The approximate Wishart distribution from Hamimeche & Lewis (2008) accounts for the non-Gaussian nature of the low-ℓ power spectra while explicitly accounting for any residual E-B correlation in the fiducial covariance matrix $\boldsymbol{M}_f$.

Because calls to `CAMB` are computationally expensive, with each call taking $\mathcal{O}(1\ {\rm s})$, we have written a code `clee-fast`[11] that linearly interpolates between precomputed power spectra, only allowing variation in r, A_s, and τ. This is similar in spirit to `PICO` (Fendt & Wandelt 2007), but works better for our purposes because it only allows variation of three parameters, reducing numerical noise and computational cost. Examples of the approximated theory curves and pseudo-C_ℓ estimates are displayed in Figure 2, and the corresponding corner plot of the parameter chain is displayed in Figure 3.

4. Predicting Parameter Constraints

We obtain sample variance limited constraints that are on the order of $\sigma_\tau/\tau \sim 5\%$. This is a factor of $\sim$3 improvement on the *Planck* precision of $\sigma_\tau/\tau \sim 16\%$, and is a factor of two away from the full-sky cosmic variance precision, $\sigma_\tau/\tau \sim 2.5\%$. We note that there exists a publicly available code, `cmb4cast` (Errard et al. 2016), that uses Fisher matrix analyses to make similar projections. This code gives $\sigma_\tau = 0.0035$, slightly larger

[11] https://github.com/pqrs6/clee-fast (Watts 2017).

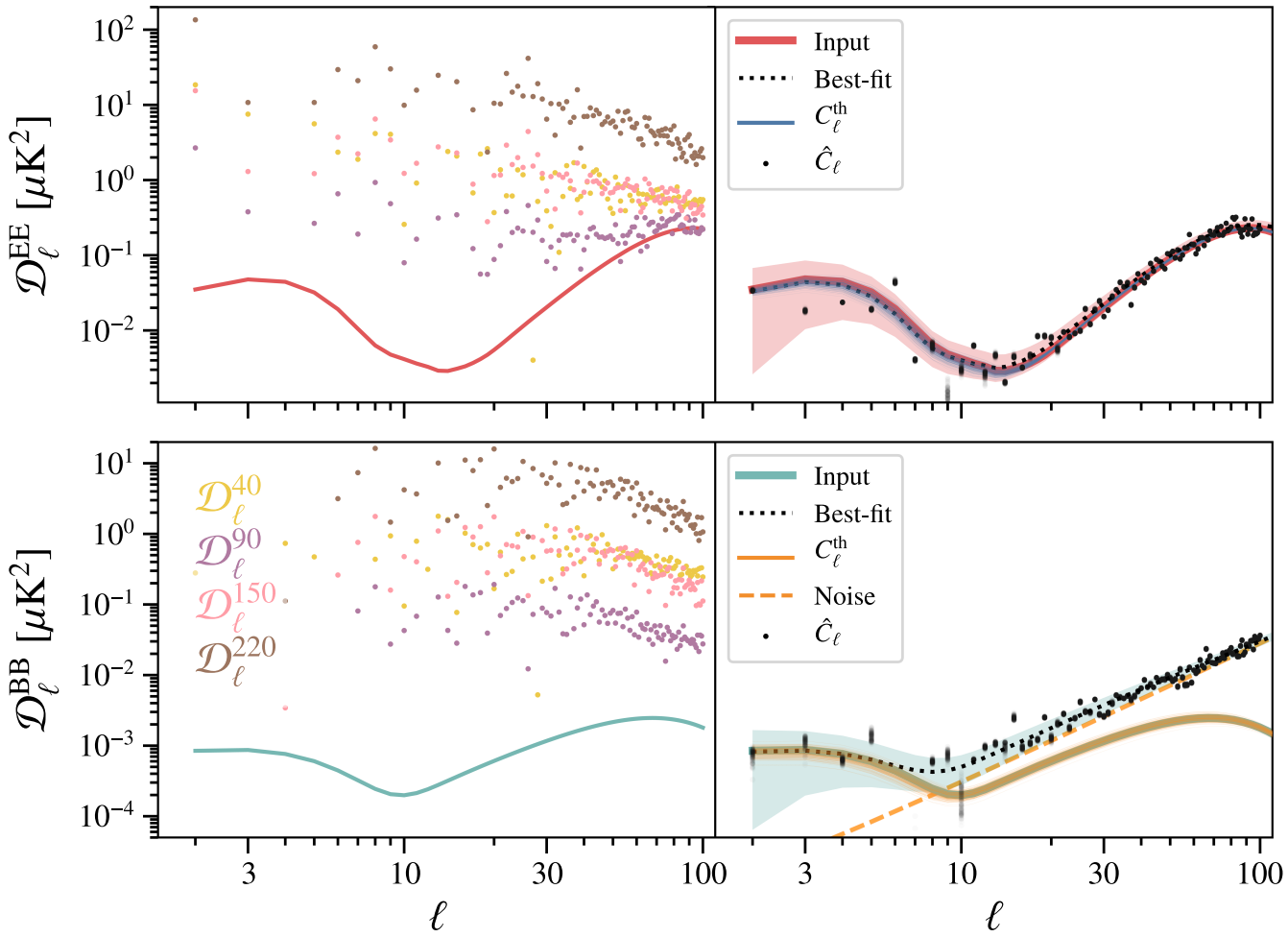

Figure 2. Left: the points labeled $\mathcal{D}_\ell^\nu \equiv \ell(\ell+1)C_\ell^\nu/2\pi$ are the autospectra associated with each CLASS band. The amplitudes of these spectra depend both on the foreground amplitudes and the inherent noise bias in autospectra. In our likelihood, we include these autospectra and the cross-spectra (not plotted) and recover the input model (solid lines) by taking linear combinations of these 16 spectra. Note that the theoretical curves have been smoothed with a $1^\circ.5$ Gaussian window function. The B-mode spectrum includes contributions from primordial gravitational waves and gravitational lensing, the latter of which is subdominant for our fiducial value of $r = 0.05$, but is dominant at the recombination peak when $r \lesssim 0.01$. Right: this is a representation of the constraining power of CLASS in pseudo-C_ℓ space with each point and line being an independent draw from the MCMC chain. The transparent overlapping gray dots ($\hat{C}_\ell$) represent estimates of the best-fit foreground-cleaned power spectrum $\sum_{\nu_1,\nu_2} c_{\nu_1} c_{\nu_2} \hat{C}_\ell^{\nu_1\times\nu_2}$ (with darker dots being many overlapping gray dots), the thin lines ($C_\ell^{\rm th}$) represent theory curves that were drawn from the chain, and the thick solid lines (Input) the input theory power spectra. The white noise level (Noise) is plotted as an orange dashed line, and the best-fit Theory + Noise power spectrum is plotted as the black dotted line. The expected error is represented by the transparent red and blue swaths, and is given in terms of the input theory spectrum and the best-fit noise, $\sigma_\ell = \sqrt{\frac{2}{(2\ell+1)f_{\rm sky}}}\,[C_\ell + N_\ell(c_\nu)]$. The input $r = 0.05$, $\log 10^{10} A_s = 3.046$, and $\tau = 0.0596$, are all recovered within 95% confidence levels.

than our $\sigma_\tau = 0.0029$. This discrepancy comes from a number of different assumptions between the codes, such as the level of foreground variation, priors on foreground variation, and the fiducial cosmological parameters. Despite these differences, it is reassuring that these different approaches yield this level of agreement.

While large-scale polarization measurements are weakly sensitive to variations in A_s, the strong E-mode sensitivity to τ can break the partial degeneracy in the well-constrained parameter combination $A_s e^{-2\tau}$ found in intensity measurements. The amplitude of primordial scalar fluctuations A_s can be used to predict the amplitude of matter fluctuations at low redshifts in the linear regime, typically parameterized by the amplitude of dark matter density fluctuations at a scale of $8\,h^{-1}$ Mpc, σ_8.

In standard ΛCDM, there are three neutrino species, and there is experimental evidence that there is a nonzero difference in the squares of each neutrino species' mass, which is detected via the oscillation of neutrinos from one species to another as they travel through space (Athanassopoulos et al. 1998; Abazajian et al. 2015). In the normal hierarchy, the mass of one neutrino is much greater than the other two, which requires that the sum of the neutrino masses $\sum m_\nu > 60$ meV. In the inverted hierarchy, two neutrinos have similar masses that are much larger than the third, which requires $\sum m_\nu > 100$ meV (Patrignani 2016, Section 14.2).

In the early universe, before neutrinos became nonrelativistic matter, massive neutrinos at small scales free streamed, effectively reducing the amplitude of matter fluctuations (Bond & Szalay 1983; Hu & Sugiyama 1996). In this way the neutrino mass affects the cosmological model's prediction for σ_8 given A_s. This effect can be used to constrain the mass of neutrinos from above, with current upper limits $\sum m_\nu < 170$ meV at the 95% C.L. using *Planck* temperature and low-ℓ polarization measurements, in combination with BOSS DR12 BAO data and the JLA Type Ia SNe catalog (Couchot et al. 2017). Tighter

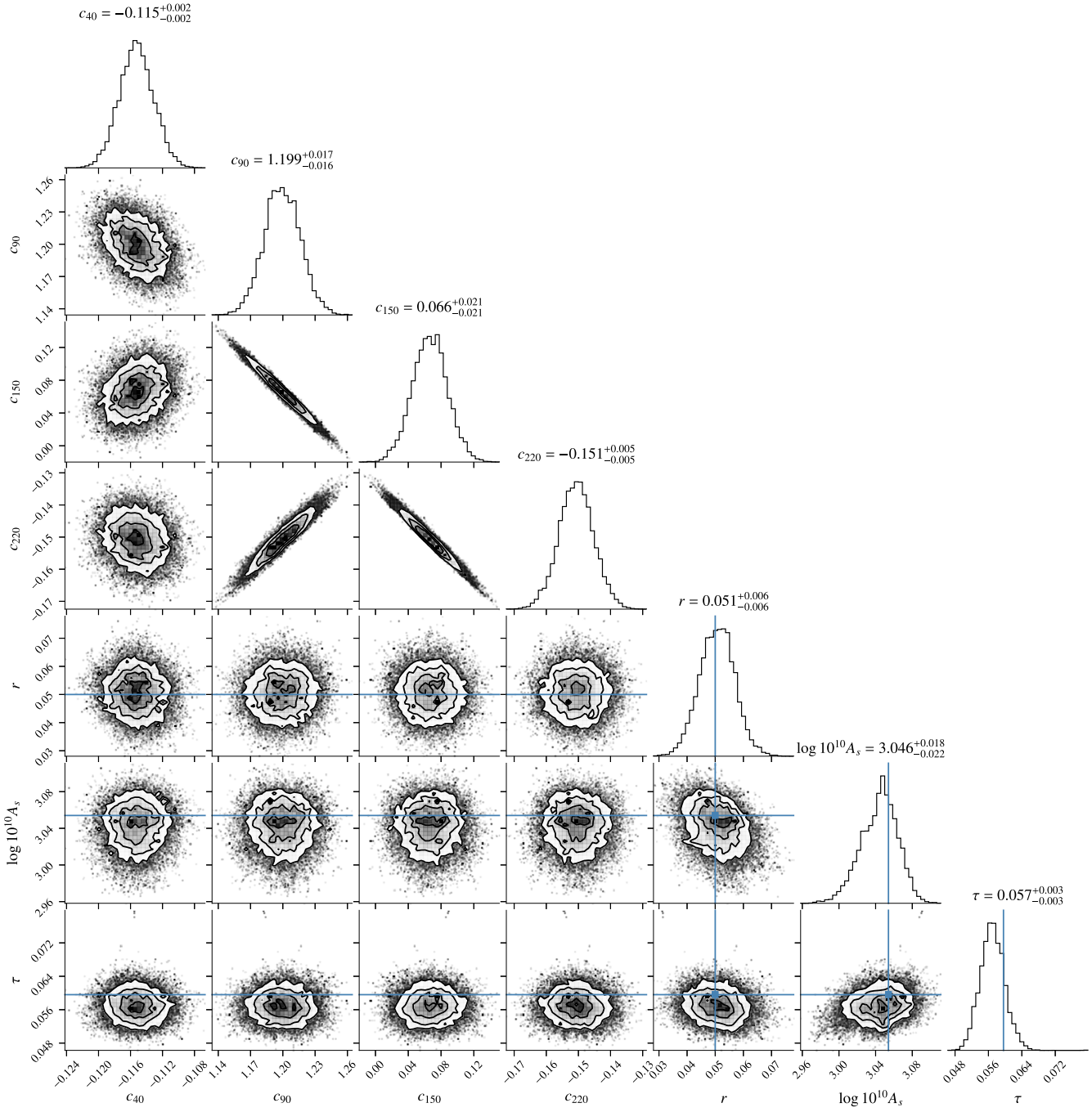

Figure 3. Monte Carlo Chain for a single simulation. All parameter fluctuations are representative of the spread found in our suite of simulations. The $\sim 1\sigma$ offset in τ is not unexpected for this single realization. An accurate and unbiased τ results from many simulations. The medians and their asymmetric 68% confidence levels are quoted above each one-dimensional histogram. The cosmological parameters are uncorrelated with the linear combination coefficients c_ν, implying that any residual foregrounds do not affect parameter constraints.

constraints on σ_8 should improve these limits, although the latest results from the Dark Energy Survey (DES, DES Collaboration et al. 2017) using galaxy clustering and weak lensing show that adding these data to the *Planck*+JLA+BAO data actually increases the 95% C.L. by 20%, which can be attributed to the tension in the values of σ_8 inferred by *Planck* and DES. There is enough uncertainty in A_s, mainly due to the partial degeneracy in $A_s e^{-2\tau}$, to weaken any $\sum m_\nu$ measurement to the $\sim 2\sigma$ level for the minimal $\sum m_\nu = 60$ meV scenario allowed by neutrino oscillations.

Allison et al. (2015) use Fisher forecasts of future measurements to predict the constraints from combining low-ℓ polarization measurements with the Dark Energy Spectroscopic Instrument (DESI) and CMB-S4. In particular, using $\ell_{\rm min} = 50$ for CMB-S4 yields $\sigma_{\sum m_\nu} \sim 27$ meV with only *WMAP* low-ℓ polarization data, and 19 meV, using pre-2016 *Planck* low-ℓ polarization sensitivities. These upper limits are inflated by uncertainty in A_s from the partial degeneracy with τ. Therefore, an external constraint on τ can break this degeneracy, allowing for any differences between the A_s

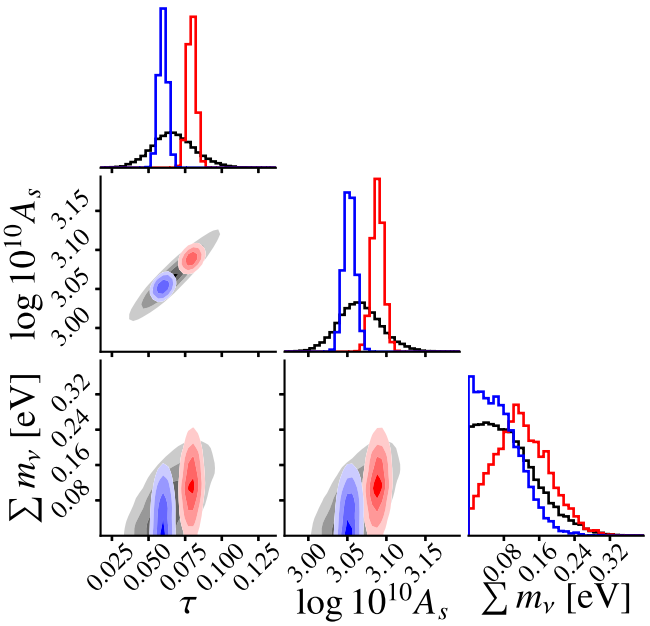

Figure 4. Combination with the *Planck* MCMC chains `base_mnu_plikHM_TTTEEE_lowTEB_lensing_BAO`, with CLASS posteriors applied using $\tau = 0.060 \pm 0.003$ (blue) and $\tau = 0.080 \pm 0.003$ (red). These two cases give neutrino mass constraints $\sum m_\nu = 64^{+56}_{-45}$ meV (blue) and $\sum m_\nu = 117 \pm 60$ meV (red). The black contours are from the raw *Planck* chains, and yield constraints $\tau = 0.067^{+0.015}_{-0.014}$ and $\sum m_\nu = 88^{+73}_{-55}$ meV.

prediction of σ_8 and the measured value of σ_8 to be directly and precisely computed. In the case of putative CMB-S4 measurements with $\ell_{\rm min} = 5$, $\sigma_{\sum m_\nu}$ is reduced to 15 meV, with the reduction in uncertainty coming almost entirely from the uncertainty on τ reducing to $\sigma_\tau = 0.003$. As we have shown, if CLASS is able to measure $C_\ell^{\rm EE}$ and $C_\ell^{\rm BB}$ down to $\ell = 2$ with white noise, it will achieve this σ_τ. In Figure 4, using *Planck* MCMC chains from the 2015 data release,[12] we show how a CLASS τ measurement would improve constraints on $\sigma_{\sum m_\nu}$ with currently available data.

5. Conclusions

We have implemented a $\hat{C}_\ell$-based likelihood for large-scale polarized CMB measurements in the presence of polarized foregrounds and instrumental noise measured on a partial sky. To do this, we implemented a fast interpolation scheme for retrieving $C_\ell(r, A_s, \tau)$, and used `PolSpice` to develop a pseudo-C_ℓ likelihood that takes into account mode coupling from a cut-sky analysis.

1. We recover the input reionization optical depth with $\sigma_\tau \sim 0.003$, within a factor of two of the cosmic variance limited case.
2. We recover the tensor-to-scalar ratio with $\sigma_r \sim 0.006$, consistent with our partial pixel-based method in Watts et al. (2015).
3. We demonstrate the power of a τ prior on massive neutrino constraints $\sum m_\nu$ using *Planck* Monte Carlo chains.

The CLASS experiment was designed to characterize the large-scale polarized CMB up to a sensitivity that allows a 2σ measurement of primordial gravitational waves with an amplitude of $r = 0.01$. As we have demonstrated, satisfying this requirement by measuring $C_\ell^{\rm EE}$ and $C_\ell^{\rm BB}$ down to $\ell = 2$ necessarily yields an estimate of the reionization optical depth τ that is limited only by sample variance and cannot be meaningfully improved upon using measurements of the CMB alone. CLASS's τ constraint will be critical in characterizing neutrino mass, helping to fulfill a major objective in both the particle physics and cosmology communities.

We acknowledge the National Science Foundation Division of Astronomical Sciences for their support of CLASS under grant Nos. 0959349, 1429236, 1636634, and 1654494. The CLASS project employs detector technology developed under several previous and ongoing NASA grants. Detector development work at JHU was funded by NASA grant number NNX14AB76A. K.H. is supported by the NASA Space Technology Research Fellowship grant number NXX14AM49H. We further acknowledge the very generous support of Jim and Heather Murren (JHU A&S '88), Matthew Polk (JHU A&S Physics BS '71), David Nicholson, and Michael Bloomberg (JHU Engineering '64). CLASS is located in the Parque Astronómica Atacama in northern Chile under the auspices of the Comisión Nacional de Investigación Científica y Tecnológica de Chile (CONICYT). Some of the results in this paper have been derived using the `HEALPix` (Górski et al. 2005) package. We also acknowledge use of the *Planck* Legacy Archive. *Planck* is an ESA science mission with instruments and contributions directly funded by ESA Member States, NASA, and Canada. Part of this research project was conducted using computational resources at the Maryland Advanced Research Computing Center (MARCC). D.J.W. thanks Graeme Addison and Janet Weiland for productive conversations, and Kirill Tchernyshyov for engaging in fruitful discussions regarding statistics. We also thank the anonymous referee for helpful comments that improved our final manuscript.

Software: `python`, `IPython` (Pérez & Granger 2007), `numpy` (van der Walt et al. 2011), `scipy` (Jones et al. 2001), `matplotlib` (Hunter 2007), `healpy` (Górski et al. 2005), `mpi4py` (Dalcín et al. 2011), `corner` (Foreman-Mackey 2016), `emcee` (Foreman-Mackey et al. 2013), `PolSpice` (Chon et al. 2004), `camb` (Lewis et al. 2000).

Appendix
Derivation of Pseudo-C_ℓ Likelihood

In Hamimeche & Lewis (2008), the cut-sky approximation for a pseudo-C_ℓ likelihood is derived assuming a fixed power spectrum estimate. However, by the nature of the joint cosmological parameter and foreground cleaning estimates, this is not accurate for our purposes, and the best-fit solution ends up being one where the total noise level is increased without bound. Here we review the calculations of Hamimeche & Lewis while keeping the dependence of the estimated $\hat{C}_\ell$ explicit.

The spherical harmonic coefficient vector $\boldsymbol{a}_{\ell m} = (a^{\rm T}_{\ell m}, a^{\rm E}_{\ell m}, a^{\rm B}_{\ell m})^T$ is a normally distributed random variable with covariance matrix at each ℓ

$$\boldsymbol{C}_\ell \equiv \langle \boldsymbol{a}_{\ell m} \boldsymbol{a}^\dagger_{\ell m} \rangle \tag{11}$$

and estimator

$$\hat{\boldsymbol{C}}_\ell \equiv \frac{1}{2\ell + 1} \sum_m \boldsymbol{a}_{\ell m} \boldsymbol{a}^\dagger_{\ell m}. \tag{12}$$

[12] `COM_CosmoParams_fullGrid_R2.00.tar.gz` from the *Planck* Legacy Archive https://pla.esac.esa.int/pla/.

In standard ΛCDM, the $\boldsymbol{a}_{\ell m}$ are Gaussian distributed with

$$-2\ln P(\{\boldsymbol{a}_{\ell m}\}|\boldsymbol{C}_\ell) = \sum_m [\boldsymbol{a}_{\ell m}^\dagger \boldsymbol{C}_\ell^{-1} \boldsymbol{a}_{\ell m} + \ln|2\pi \boldsymbol{C}_\ell|]$$
$$= (2\ell+1)(\mathrm{Tr}[\hat{\boldsymbol{C}}_\ell \boldsymbol{C}_\ell^{-1}] + \ln|\boldsymbol{C}_\ell|) + \mathrm{const.} \quad (13)$$

For a full-sky likelihood, $\hat{\boldsymbol{C}}_\ell$ contains all of the sky's information, and is drawn from a Wishart distribution,

$$P(\hat{\boldsymbol{C}}_\ell|\boldsymbol{C}_\ell) \propto \frac{|\hat{\boldsymbol{C}}_\ell|^{(2\ell-n)/2}}{|\boldsymbol{C}_\ell|^{(2\ell+1)/2}} e^{-(2\ell+1)\mathrm{Tr}(\hat{\boldsymbol{C}}_\ell \boldsymbol{C}_\ell^{-1})/2}, \quad (14)$$

where n is the number of fields considered. We take $n = 2$ for $a_{\ell m}^{\mathrm{E}}$ and $a_{\ell m}^{\mathrm{B}}$.

The root of the Hamimeche & Lewis approximation involves rewriting this likelihood in a quadratic form. Using orthogonal $\boldsymbol{U}_\ell$ and diagonal $\boldsymbol{D}_\ell$ to rewrite $\boldsymbol{C}_\ell^{-1/2} \hat{\boldsymbol{C}}_\ell \boldsymbol{C}_\ell^{-1/2} \equiv \boldsymbol{U}_\ell \boldsymbol{D}_\ell \boldsymbol{U}_\ell^T$, the probability can be written as

$$-2\ln P = (2\ell+1)\left\{\mathrm{Tr}[\hat{\boldsymbol{C}}_\ell \boldsymbol{C}_\ell^{-1}] + \ln|\boldsymbol{C}_\ell| - \frac{2\ell-n}{2\ell+1}\ln|\hat{\boldsymbol{C}}_\ell|\right\} + \mathrm{const.} \quad (15)$$

$$= (2\ell+1)\{\mathrm{Tr}[\hat{\boldsymbol{C}}_\ell \boldsymbol{C}_\ell^{-1}] - \ln|\hat{\boldsymbol{C}}_\ell \boldsymbol{C}_\ell^{-1}| - n\} + n[\ln|\hat{\boldsymbol{C}}_\ell| + 2\ell + 1] + \mathrm{const.} \quad (16)$$

$$= \frac{2\ell+1}{2}\mathrm{Tr}\,[\boldsymbol{G}(\boldsymbol{D}_\ell)]^2 + n\ln|\hat{\boldsymbol{C}}_\ell| + \mathrm{const.}, \quad (17)$$

where $G(x) \equiv \sqrt{2(x - \ln x - 1)}$ and $[\boldsymbol{G}(\boldsymbol{D}_\ell)]_{ij} = G(D_{\ell,ii})\delta_{ij}$.

Note that, in Equation (15), if we assume that $\hat{\boldsymbol{C}}_\ell$ is constant, we can adjust the constant such that $-2\ln P = 0$ when $\boldsymbol{C}_\ell = \hat{\boldsymbol{C}}_\ell$. This is where our derivation differs from Hamimeche & Lewis. From here, the derivation in Hamimeche & Lewis applies, carrying along the extra $n\ln|\hat{\boldsymbol{C}}_\ell|$ term. This term essentially adds a penalty for increasing the noise, preventing the coefficients in $\hat{\boldsymbol{C}}_\ell = \sum_{\nu_1,\nu_2} c_{\nu_1} c_{\nu_2} \hat{\boldsymbol{C}}_\ell^{\nu_1\times\nu_2}$ from getting too large.

ORCID iDs

Duncan J. Watts https://orcid.org/0000-0002-5437-6121
Bingjie Wang (王冰洁) https://orcid.org/0000-0001-9269-5046
John W. Appel https://orcid.org/0000-0002-8412-630X
Charles L. Bennett https://orcid.org/0000-0001-8839-7206
David T. Chuss https://orcid.org/0000-0003-0016-0533
Sumit Dahal (सुमित दाहाल) https:/orcid.org/0000-0002-1708-5464
Joseph R. Eimer https://orcid.org/0000-0001-6976-180X
Thomas Essinger-Hileman https://orcid.org/0000-0002-4782-3851
Matthew Petroff https://orcid.org/0000-0002-4436-4215
Edward J. Wollack https://orcid.org/0000-0002-7567-4451
Zhilei Xu (徐智磊) https://orcid.org/0000-0001-5112-2567

References

Abazajian, K. N., Adshead, P., Ahmed, Z., et al. 2016, arXiv:1610.02743
Abazajian, K. N., Arnold, K., Austermann, J., et al. 2015, APh, 63, 66
Addison, G. E., Huang, Y., Watts, D. J., et al. 2016, ApJ, 818, 132
Aiola, S., Amico, G., Battaglia, P., et al. 2012, Proc. SPIE, 8446, 84467
Albrecht, A., & Steinhardt, P. J. 1982, PhRvL, 48, 1220
Allison, R., Caucal, P., Calabrese, E., Dunkley, J., & Louis, T. 2015, PhRvD, 92, 123535
Athanassopoulos, C., Auerbach, L. B., Burman, R. L., et al. 1998, PhRvL, 81, 1774
Austermann, J. E., Aird, K. A., Beall, J. A., et al. 2012, Proc. SPIE, 8452, 84521
Bennett, C. L., Larson, D., Weiland, J. L., et al. 2013, ApJS, 208, 20
Bond, J. R., & Szalay, A. S. 1983, ApJ, 274, 443
Chon, G., Challinor, A., Prunet, S., Hivon, E., & Szapudi, I. 2004, MNRAS, 350, 914
Chuss, D. T., Wollack, E. J., Henry, R., et al. 2012, ApOpt, 51, 197
Couchot, F., Henrot-Versillé, S., Perdereau, O., et al. 2017, A&A, 606, A104
Dalcín, L. D., Paz, R. R., Kler, P. A., & Cosimo, A. 2011, AdWR, 34, 1124
DES Collaboration, Abbott, T. M. C., Abdalla, F. B., et al. 2017, arXiv:1708.01530
Eimer, J. R., Bennett, C. L., Chuss, D. T., et al. 2012, Proc. SPIE, 8452, 845220
Einhorn, M. B., & Sato, K. 1981, NuPhB, 180, 385
Errard, J., Feeney, S. M., Peiris, H. V., & Jaffe, A. H. 2016, JCAP, 2016, 052
Essinger-Hileman, T., Ali, A., Amiri, M., et al. 2014, Proc. SPIE, 9153, 91531
Fan, X., Strauss, M. A., Becker, R. H., et al. 2006, AJ, 132, 117
Fendt, W. A., & Wandelt, B. D. 2007, ApJ, 654, 2
Foreman-Mackey, D. 2016, JOSS, 24
Foreman-Mackey, D., Hogg, D. W., Lang, D., & Goodman, J. 2013, PASP, 125, 306
Fuskeland, U., Wehus, I. K., Eriksen, H. K., & Næss, S. K. 2014, ApJ, 790, 104
Galli, S., Benabed, K., Bouchet, F., et al. 2014, PhRvD, 90, 063504
Gandilo, N. N., Ade, P. A. R., Benford, D., et al. 2016, Proc. SPIE, 9914, 99141J
Górski, K. M., Hivon, E., Banday, A. J., et al. 2005, ApJ, 622, 759
Gunn, J. E., & Peterson, B. A. 1965, ApJ, 142, 1633
Guth, A. H. 1981, PhRvD, 23, 347
Hamimeche, S., & Lewis, A. 2008, PhRvD, 77, 103013
Harrington, K., Marriage, T., Ali, A., et al. 2016, Proc. SPIE, 9914, 99141K
Heinrich, C. H., Miranda, V., & Hu, W. 2017, PhRvD, 95, 023513
Henning, J. W., Sayre, J. T., Reichardt, C. L., et al. 2018, ApJ, 852, 97
Hu, W., & Okamoto, T. 2004, PhRvD, 69, 043004
Hu, W., & Sugiyama, N. 1996, ApJ, 471, 542
Hunter, J. D. 2007, CSE, 9, 90
Jones, E., Oliphant, T., Peterson, P., et al. 2001, SciPy: Open Source Scientific Tools for Python, http://www.scipy.org/
Kamionkowski, M., Kosowsky, A., & Stebbins, A. 1997, PhRvD, 55, 7368
Kazanas, D. 1980, ApJL, 241, L59
Krachmalnicoff, N., Baccigalupi, C., Aumont, J., Bersanelli, M., & Mennella, A. 2016, A&A, 588, A65
Leenaarts, J., Golding, T., Carlsson, M., Libbrecht, T., & Joshi, J. 2016, A&A, 594, A104
Lewis, A., Challinor, A., & Lasenby, A. 2000, ApJ, 538, 473
Linde, A. D. 1982, PhLB, 108, 389
Liu, A., Pritchard, J. R., Allison, R., et al. 2016, PhRvD, 93, 043013
Louis, T., Grace, E., Hasselfield, M., et al. 2017, JCAP, 6, 031
Mangilli, A., Plaszczynski, S., & Tristram, M. 2015, MNRAS, 453, 3174
Miller, N. J., Chuss, D. T., Marriage, T. A., et al. 2016, ApJ, 818, 151
Mukhanov, V. F., & Chibisov, G. V. 1981, JETPL, 33, 532
Page, L., Hinshaw, G., Komatsu, E., et al. 2007, ApJS, 170, 335
Patrignani, C. 2016, ChPhC, 40, 100001
Pérez, F., & Granger, B. E. 2007, CSE, 9, 21
Planck Collaboration, Adam, R., Ade, P.A.R., et al. 2016b, A&A, 594, A10
Planck Collaboration, Adam, R., Aghanim, N., et al. 2016a, A&A, 596, A108
Planck Collaboration, Ade, P.A.R., Aghanim, N., et al. 2016c, A&A, 594, A13
Planck Collaboration, Aghanim, N., Ashdown, M., et al. 2016d, A&A, 596, A107
Planck Collaboration, Aghanim, N., Ashdown, M., et al. 2017, A&A, 599, A51
Planck Collaboration, Akrami, Y., Ashdown, M., et al. 2018, arXiv:1801.04945
Seljak, U., & Zaldarriaga, M. 1997, PhRvL, 78, 2054
Sheehy, C., & Slosar, A. 2018, PhRvD, 97, 043522
Smith, K. M., & Zaldarriaga, M. 2007, PhRvD, 76, 043001
Starobinsky, A. A. 1980, PhLB, 91, 99
Suzuki, A., Ade, P., Akiba, Y., et al. 2016, JLTP, 184, 805
Tajima, O., Choi, J., Hazumi, M., et al. 2012, Proc. SPIE, 8452, 84521
Thorne, B., Dunkley, J., Alonso, D., & Næss, S. 2017, MNRAS, 469, 2821
Thornton, R. J., Ade, P. A. R., Aiola, S., et al. 2016, ApJS, 227, 21
van der Walt, S., Colbert, S. C., & Varoquaux, G. 2011, CSE, 13, 22
Watts, D. J. 2017, clee_fast, Zenodo, doi:10.5281/zenodo.1066547
Watts, D. J., Larson, D., Marriage, T. A., et al. 2015, ApJ, 814, 103
Weiland, J. L., Osumi, K., Addison, G. E., et al. 2018, arXiv:1801.01226
Wu, W. L. K., Ade, P. A. R., Ahmed, Z., et al. 2016, JLTP, 184, 765